Development 137, 1645-1655 (2010) doi:10.1242/dev.044107

The PAR complex regulates pulsed actomyosin contractions during amnioserosa apical constriction in *Drosophila*

Daryl J. V. David, Alisa Tishkina and Tony J. C. Harris*

SUMMARY

Apical constriction is a major mechanism underlying tissue internalization during development. This cell constriction typically requires actomyosin contractility. Thus, understanding apical constriction requires characterization of the mechanics and regulation of actomyosin assemblies. We have analyzed the relationship between myosin and the polarity regulators Par-6, aPKC and Bazooka (Par-3) (the PAR complex) during amnioserosa apical constriction at *Drosophila* dorsal closure. The PAR complex and myosin accumulate at the apical surface domain of amnioserosa cells at dorsal closure, the PAR complex forming a patch of puncta and myosin forming an associated network. Genetic interactions indicate that the PAR complex supports myosin activity during dorsal closure, as well as during other steps of embryogenesis. We find that actomyosin contractility in amnioserosa cells is based on the repeated assembly and disassembly of apical actomyosin networks, with each assembly event driving constriction of the apical domain. As the networks assemble they translocate across the apical patch of PAR proteins, which persist at the apical domain. Through loss- and gain-of-function studies, we find that different PAR complex components regulate distinct phases of the actomyosin assembly/disassembly cycle: Bazooka promotes the duration of actomyosin pulses and Par-6/aPKC promotes the lull time between pulses. These results identify the mechanics of actomyosin contractility that drive amnioserosa apical constriction and how specific steps of the contractile mechanism are regulated by the PAR complex.

KEY WORDS: PAR proteins, Myosin, Apical constriction, Amnioserosa, *Drosophila*

INTRODUCTION

Epithelial morphogenesis is driven by various cellular processes, including changes to cell shape, cell-cell interactions and cell numbers. Polarized changes to cell shape and cell-cell interactions are often driven by actomyosin contractility generated by actin and non-muscle myosin II (henceforth myosin). Actomyosin contractility drives apical constriction and invagination of the vertebrate neural tube and the *Drosophila* ventral furrow (reviewed by Lecuit and Lenne, 2007) and cell ingression in *C. elegans* (reviewed by Cowan and Hyman, 2007). It also drives cell intercalation and convergent extension in the *Drosophila* germband (reviewed by Lecuit and Lenne, 2007; Zallen, 2007) and in *Xenopus* (Skoglund et al., 2008). Additionally, supracellular actomyosin cables function in *Drosophila* dorsal closure (DC) (reviewed by Jacinto et al., 2002) and in *C. elegans* embryo elongation (Simske and Hardin, 2001). To understand such morphological changes, we must define the mechanics of actomyosin assemblies and their regulation.

Par-6, aPKC and Bazooka (Baz; Par-3) are major regulators of apical polarity. They can function as a complex and also separately, with Par-6 and aPKC typically acting together and the scaffold protein Baz functioning apart (reviewed by Goldstein and Macara, 2007; Suzuki and Ohno, 2006). They regulate asymmetric cell divisions, the positioning of cellular junctions, cell migration and axon outgrowth (reviewed by Goldstein and Macara, 2007; Munro, 2006; Wiggin et al., 2005; Wodarz and Nathke, 2007), but few links to actomyosin contractility are known. In *C. elegans*, the PAR complex regulates apical myosin accumulation during cell ingression (Nance et al., 2003) and actomyosin flows in the one-cell embryo (Munro et al., 2004). In *Drosophila*, the PAR complex promotes apical myosin accumulation in egg chamber follicle cells (Wang and Riechmann, 2007). In these examples, PAR proteins and myosin localize to the same regions of the cell. By contrast, Baz and myosin have mutually exclusive planar polarized distributions in the *Drosophila* germband (Zallen and Wieschaus, 2004).

The *Drosophila* amnioserosa provides an excellent model of tissue morphogenesis. It undergoes two types of morphogenesis during embryogenesis. First, the squamous tissue forms from a columnar epithelium at gastrulation. During this process, Baz and myosin display the same, reciprocal, planar polarized pattern as in the germband, but are gradually lost from the cortex as the amnioserosa flattens (Pope and Harris, 2008). The loss of apical contractility appears to allow microtubules and other factors to extend and flatten the apical domain, generating a squamous epithelium on the dorsal surface of the embryo during gastrulation (Pope and Harris, 2008). The second major change to the amnioserosa occurs at DC, when the surrounding epidermis closes over the amnioserosa, which is internalized and degraded. The amnioserosa functions with the epidermis to drive DC (Kiehart et al., 2000). As the process begins, amnioserosa cells undergo rounds of constriction and relaxation (Solon et al., 2009). The cells display apical myosin, and expressing myosin solely in the amnioserosa of myosin mutants is sufficient to rescue amnioserosa cell constriction and overall DC (Franke et al., 2005). The epidermis normally also plays a role, forming a supracellular ring of actomyosin that surrounds the amnioserosa and promotes closure (Franke et al., 2005; Kiehart et al., 2000; Rodriguez-Diaz et al., 2008; Solon et al., 2009). The leading edge actomyosin ring is well studied (reviewed by Harden, 2002; Jacinto et al., 2002), but the mechanics and regulation of amnioserosa actomyosin contractility are ill defined.

Department of Cell and Systems Biology, University of Toronto, Toronto, ON M5S 3G5, Canada.

*Author for correspondence (tony.harris@utoronto.ca)

Accepted 3 March 2010

We analyzed associations between the PAR complex and myosin during amnioserosa morphogenesis at DC. We find that amnioserosa apical constriction is based on the repeated assembly and disassembly of apical actomyosin networks. As the networks form, they interact transiently with an apical PAR protein patch. Remarkably, different PAR proteins regulate distinct phases of the actomyosin assembly/disassembly cycle.

MATERIALS AND METHODS

Fly stocks

zip::GFP and *baz::GFP* were GFP gene traps into endogenous loci (FlyTrap, flytrap.med.yale.edu). *MoeABD-GFP* (Kiehart et al., 2000), *sqh-GFP* in a null *sqh* mutant background (Royou et al., 2002), *sqh::mCherry* (Martin et al., 2009), *UAS-par-6* (Pinheiro and Montell, 2004), *UAS-aPKC::CAAX* (Sotillos et al., 2004) and *UAS-baz* (M. Pellikka and U. Tepass, University of Toronto, Canada) were gifts. *UAS-par-6::GFP* was generated with standard molecular methods and inserted into the genome by P-element insertion (Genetic Services). *arm::CFP* and *UAS-baz::mCherry* were generated previously (McGill et al., 2009; Pope and Harris, 2008). For visualization, UAS constructs were expressed zygotically using *Actin-5C-GAL4* [Bloomington *Drosophila* Stock Center (BDSC) #3954]. For perturbation studies, UAS constructs were specifically expressed in the amnioserosa using 332.3-*GAL4* (BDSC). baz^{Xi106} mutants (A. Wodarz, University of Göttingen, Germany) and $par\text{-}6^{\Delta 226}$ and $aPKC^{K06403}$ mutants (C. Doe, University of Oregon, USA) were gifts. zip^{1} and zip^{2} mutants were from the BDSC. *yellow white* was used as wild type.

Cuticle preparations

Embryos were collected for 24 hours (25°C), removed from adults and allowed to develop for another 48 hours. Unhatched embryos were washed and dechorionated with 50% bleach, mounted on slides with Hoyer's mountant:lactic acid (1:1) and baked overnight (60°C).

Embryo staining

Embryos were fixed for 10 minutes in 1:1 10% formaldehyde in PBS:heptane, devitellinized by hand peeling and stained with phalloidin. For other stainings, embryos were fixed in 1:1 3.7% formaldehyde in PBS:heptane for 20 minutes and devitellinized in methanol. Blocking and staining were in PBS containing 1% goat serum and 0.1% Triton X-100. Primary antibodies used were: mouse anti-Arm [1:500; Developmental Studies Hybridoma Bank (DSHB)] and anti-Crb (1:500; DSHB); rabbit anti-Baz (1:3500); and anti-aPKC (1:2000; Santa Cruz Biotechnology); and rat anti-DE-Cad (1:100; DSHB) and anti-Par-6 (1:100; C. Doe). F-actin was stained with Alexa Fluor 568-conjugated phalloidin (1:200; Invitrogen). Secondary antibodies were conjugated with Alexa Fluor 488, 546 and 647 (Invitrogen).

Imaging

Fixed embryos were mounted in Aqua-Poly/Mount (Polysciences) and imaged with a LSM 510 confocal microscope (Carl Zeiss) at room temperature with 40× (Plan-NeoFluor, NA 1.3) and 63× (Plan-Apochromat, NA 1.4) objectives and LSM 510 AIM software. *z*-stacks had a 0.3 μm step size.

For live imaging, dechorionated embryos were mounted in halocarbon oil (series 700; Halocarbon Products) on petriPERM dishes (Sigma) and imaged with a Quorum spinning disk confocal system (Quorum Technologies) at room temperature with a 63× (Plan-Apochromat, NA 1.4) objective, a piezo top plate, a Hamamatsu EM CCD camera and using Volocity software (Improvision). *z*-stacks had a 0.3 μm step size. Autofluorescent egg shell vitelline membrane served as a marker for the apical surface of the cells lying just beneath. For quantifying DC rates, embryos were glued to coverslips, covered with halocarbon oil and imaged as above but with halocarbon oil exposed to air and with a 20× (Plan-Apochromat, NA 0.8) objective and 2 μm step sizes.

For post-acquisition image analysis and manipulation, maximum intensity projections were performed with Volocity software. Three-dimensional reconstructions were with Imaris software (Bitplane). To quantify colocalization, the apical domain was cropped to the region where proteins were enriched, and the minimum and maximum intensity values were adjusted for each channel to include only the top half of the original values (ImageJ) and the Colocalization Test plug-in was applied (ImageJ). For figure preparation, input levels were adjusted in Adobe Photoshop so that the main signal range spanned the full output grayscale, and image resizing was by bicubic interpolation (minimal changes occurred at normal magnifications).

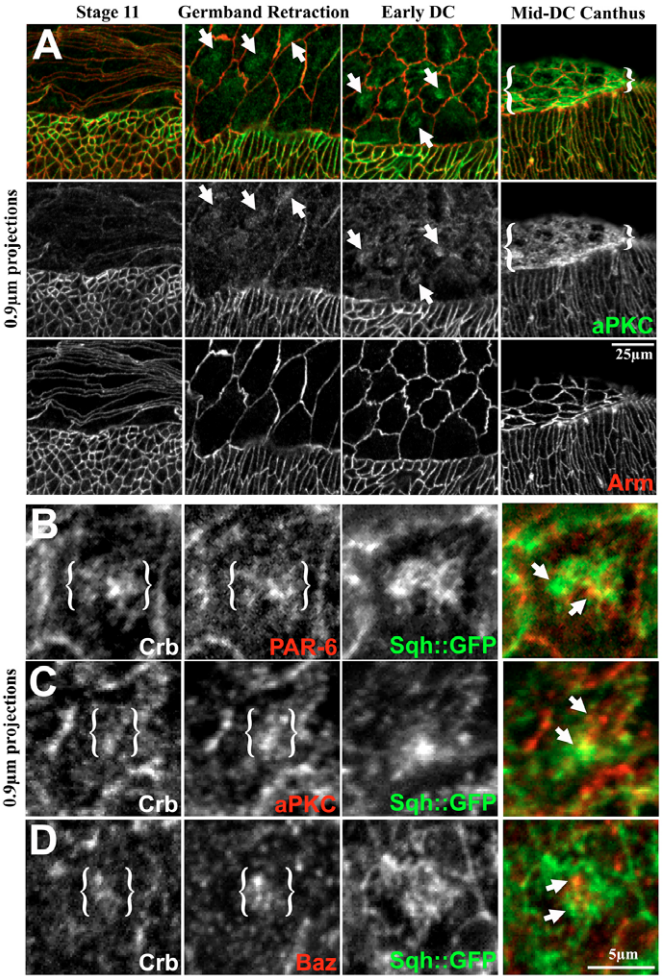

Fig. 1. The PAR complex at the apical surface of amnioserosa cells. (**A**) aPKC and Arm immunostaining of *Drosophila* embryos from stage 11 to dorsal closure (DC). Amnioserosa at top, epidermis below. Note the localization of aPKC at the apical surface (arrows/brackets). (**B-D**) Single amnioserosa cells at DC stained for PAR proteins (B, Par-6; C, aPKC; D, Baz) and Crb (B-D) in Sqh::GFP embryos. Colocalization of PAR protein with Crb is bracketed. Note the lack of local colocalization of PAR protein and myosin (Sqh, arrows).

Statistics

Comparisons were made using unpaired two-tailed *t*-tests in Excel (Microsoft).

RESULTS

A PAR protein patch forms at the apical surface of amnioserosa cells at dorsal closure

To characterize Par-6, aPKC and Baz localization in the amnioserosa after gastrulation, we immunostained wild-type *Drosophila* embryos at full germband extension, germband retraction and DC. As seen previously (Pope and Harris, 2008; Wodarz et al., 2000), Par-6, aPKC and Baz were present at lower levels at the apical circumference of amnioserosa versus epidermal cells at full germband extension (stages 9-11) (Fig. 1A shows aPKC), in contrast

to adherens junctions (AJs), which had comparable apical circumferential levels in each tissue [Fig. 1A shows Armadillo (Arm)]. From germband retraction into DC, Par-6, aPKC and Baz accumulated in a patch at the central apical surface of amnioserosa cells (Fig. 1A, arrows) and also localized around the apical circumference. AJ proteins Arm and DE-Cadherin (DE-Cad; the gene product of *shotgun*) were absent from these apical surface patches (Fig. 1A). By late DC, Par-6, aPKC and Baz covered a large proportion of the remaining apical surface (Fig. 1A, brackets). Thus, Par-6, aPKC and Baz relocalize to a specific patch at the apical surface of amnioserosa cells at germband retraction and DC.

The apical PAR protein patch associates with Crumbs and a myosin network

To assess what complexes Par-6, aPKC and Baz might form within the apical domain, we localized each protein along with the apical transmembrane protein Crumbs (Crb) (by immunostaining) and Spaghetti squash (Sqh) (by Sqh::GFP fluorescence) (Sqh encodes non-muscle myosin II regulatory light chain). High-magnification imaging revealed that the PAR protein patches include small puncta (Fig. 1B-D, brackets). Par-6 and Crb often displayed a high degree of colocalization at these puncta (Fig. 1B). aPKC and Baz only occasionally showed this high degree of colocalization with Crb (Fig. 1C,D), suggesting fixation artifacts or more dynamic interactions. Comparisons with Sqh::GFP showed that the patches of Crb, Par-6, aPKC and Baz overlapped with apical surface myosin networks, but there was little colocalization between specific puncta and nodes of the myosin networks (Fig. 1B-D, arrows). The PAR protein patches and myosin networks also had different overall shapes (Fig. 1B-D). Quantification of where the PAR protein patches and myosin networks overlapped showed that each PAR protein distribution had a significantly higher correlation with Crb than with the distribution of Sqh::GFP, although colocalization with Crb varied (Table 1). Thus, the PAR protein patches are closely linked with Crb and appear less directly associated with myosin networks.

Components of the PAR complex support myosin activity

Since amnioserosa myosin activity contributes to DC (Franke et al., 2005), we hypothesized that the PAR proteins support this activity. To test functional interactions with myosin and a role for PAR proteins in DC, we examined the terminal embryonic phenotypes of mutants using cuticle preparations. Zygotic single mutants for zip^1 (*zipper* encodes non-muscle myosin II heavy chain) are embryonic lethal and display a prominent dorsal hole due to failed DC (Fig. 2A, outlined). By contrast, zygotic single mutants for $aPKC^{K06403}$ and $par\text{-}6^{\Delta 226}$ complete embryogenesis due to maternally inherited gene product. However, $aPKC^{K06403}$, zip^1 and $par\text{-}6^{\Delta 226}$; zip^1 double mutants displayed a prominent dorsal hole merged with a large head hole (Fig. 2A, overall holes outlined, arrows mark head holes), indicating enhancement of the zip^1 phenotype. $par\text{-}6^{\Delta 226}$; $aPKC^{K06403}$, zip^1 triple mutants showed similar enhancement (Fig. 2A). All of the dead embryos from heterozygous parents were analyzed and scored (Fig. 2A′). Thus, Par-6 and aPKC support myosin activity, but specific effects on DC could not be assessed because of the severity of the zip^1 DC phenotype.

To assess effects on DC, we tested interactions between single mutants that lack DC phenotypes on their own. zip^2 zygotic single mutants lacked dorsal holes (Fig. 2B). By contrast, $par\text{-}6^{\Delta 226}$; zip^2 double mutants displayed merged dorsal and head holes (Fig. 2B, outlined). All of the dead embryos from doubly heterozygous parents were analyzed and scored (Fig. 2B′). We also tested baz^{Xi106} zygotic single mutants, most of which lacked dorsal holes (Fig. 2C). Reducing the dosage of *zip* by half in these mutants enhanced the phenotype, generating merged dorsal and head holes (Fig. 2C, outlined) and ventral holes (Fig. 2C, arrow; quantified in Fig. 2C′). Thus, genetic interactions between PAR complex components and myosin affect DC and the morphogenesis of other tissues.

Apical actin and myosin networks undergo repeated assembly/disassembly cycles in amnioserosa cells

We pursued how the PAR complex interacts with myosin in the amnioserosa at DC. First, we needed to characterize the development and activity of the myosin networks. We analyzed their development by live imaging at full germband extension, germband retraction and DC. A gene-trap line with GFP inserted into the *zip* locus (Zip::GFP) revealed little cortical myosin in the amnioserosa at full germband extension (Fig. 3A), consistent with previous observations (Pope and Harris, 2008). However, myosin networks began assembling and disassembling sporadically across the amnioserosa during germband retraction (Fig. 3B, arrows), both apically and basally. By DC, all cells displayed repeated cycles of myosin network assembly and disassembly (Fig. 3C, arrows; see

Table 1. Pearson correlation coefficients for protein colocalization at the apical surface

	Crb	Sqh::GFP	*P*-value	*n*
Par-6	0.64±0.13	0.42±0.18	4.24×10^{-8}	35
Crb		0.39±0.15		
aPKC	0.53±0.15	0.45±0.17	0.0423	29
Crb		0.36±0.14		
Baz	0.36±0.18	0.22±0.16	0.00882	18
Crb		0.27±0.14		
Actin (phalloidin)	–	0.70±0.10	–	30
		Sqh::mCherry		
Baz::GFP (live)	–	0.16±0.10	–	27
	Par-6::GFP			
Baz::mCherry (live)	0.42±0.13	–	–	36
		Sqh::mCherry		
Par-6::GFP (live)	–	0.14±0.12	–	13

Columns 2 and 3 show mean ± s.d.

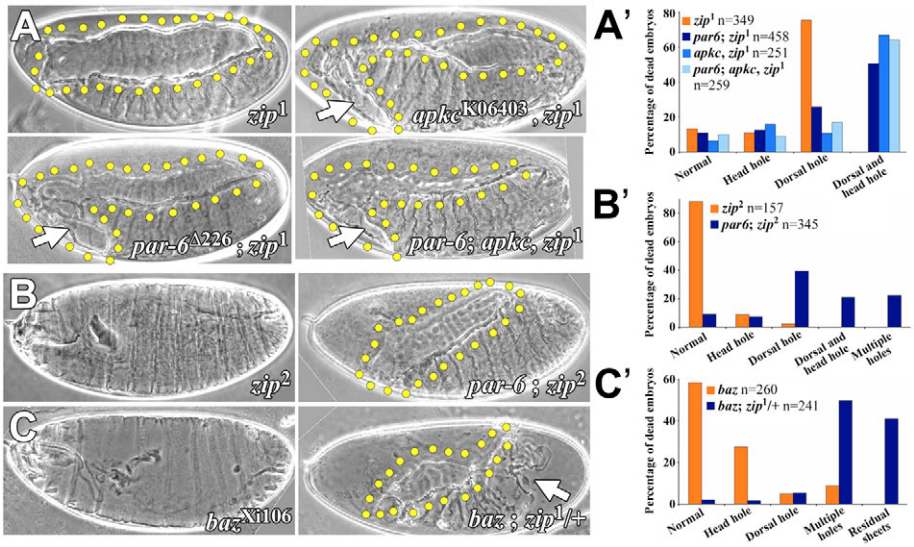

Fig. 2. Genetic interactions between PAR complex and myosin mutants. (**A**) *Drosophila zip*^{1} single-mutant cuticle with large dorsal hole (yellow dotted outline). Double and triple mutants with *par-6* and *aPKC* alleles showing dorsal holes merged with head holes (arrows). (**B**) *zip*^{2} single-mutant cuticle compared with *par-6*; *zip*^{2} double-mutant cuticle with combined dorsal and head holes (outlined). (**C**) *baz* single-mutant cuticle compared with *baz* single-mutant with half the dosage of *zip*, showing a combined dorsal and head hole (outlined) and ventral hole (arrow). (**A′-C′**) Quantification of the embryonic lethality associated with the hole phenotypes for each genotype examined.

Movie 1 in the supplementary material) that were restricted to the apical domain. Sqh::GFP displayed similar developmental changes and network behavior (data not shown).

To probe for F-actin, we imaged the F-actin-binding domain of Moesin (Moe) fused to GFP (MoeABD::GFP). MoeABD::GFP localized to circumferential cell protrusions at each developmental stage, but only displayed pulsing apical surface networks at germband retraction and DC (Fig. 3D-F, arrows). Thus, apical actin and myosin networks form with the same developmental timing as the apical PAR protein patch, and display a pulsing behavior.

To assess the link between the actin and myosin networks, we first compared them in fixed tissues. Dual imaging of Sqh::GFP and phalloidin staining (for F-actin) revealed colocalization in amnioserosa apical surface networks at DC (Fig. 3G, arrows; Table

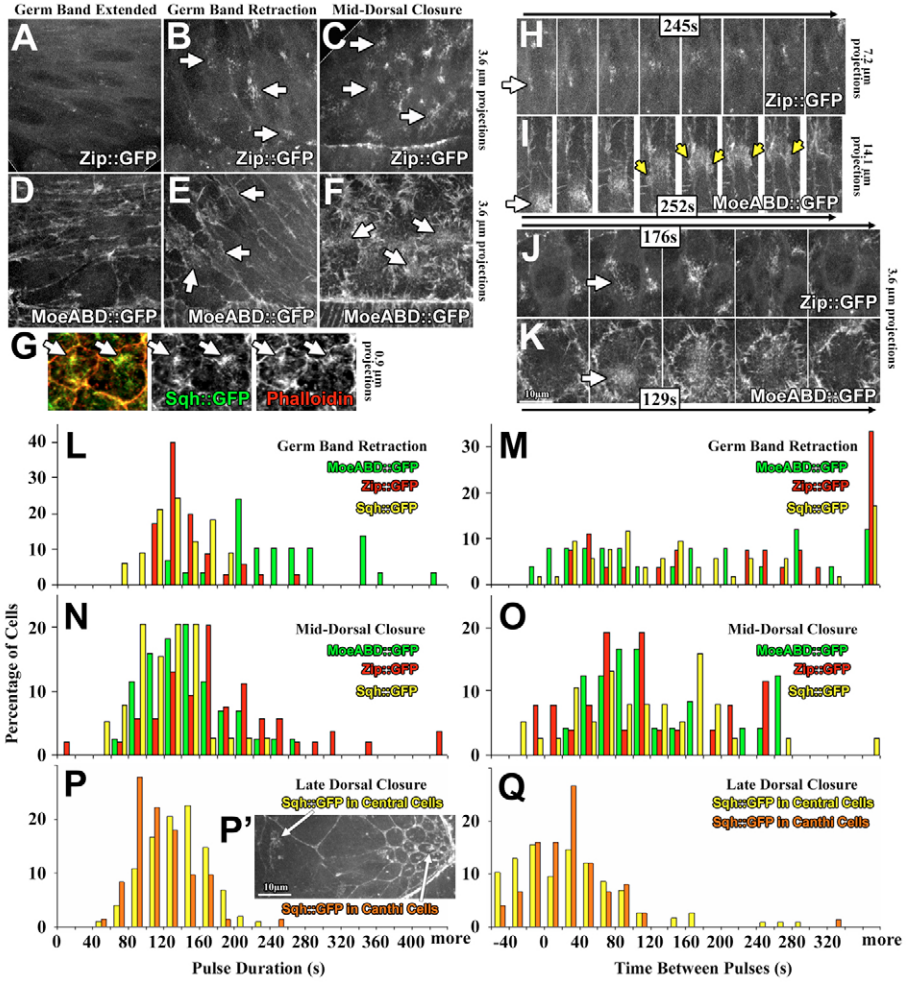

Fig. 3. Pulsing actin and myosin networks develop at the apical surface of amnioserosa cells. (**A-F**) Live imaging of *Drosophila* embryos from germband extension to DC. Arrows mark networks. (A-C) Zip::GFP. (D-F) MoeABD::GFP. (**G**) Fixed amnioserosa cells at mid-DC. The colocalization of Sqh::GFP with phalloidin (F-actin) at networks is indicated by arrows. (**H**,**I**) Zip::GFP (H, arrow) and MoeABD::GFP (I, arrow) network dynamics at germband retraction. Note the cell protrusions from the MoeABD::GFP network (yellow arrows). s, seconds. (**J**,**K**) Zip::GFP (J, arrow) and MoeABD::GFP (K, arrow) network dynamics at mid-DC. (**L-O**) Quantification of MoeABD::GFP, Zip::GFP and Sqh::GFP network durations (L,N) and lull times between pulses (M,O) at germband retraction (L,M) and mid-DC (N,O). (**P-Q**) Quantification of Sqh::GFP network dynamics (P,Q) at late DC in central versus canthi cells, as illustrated in P′.

Table 2. Actin and myosin network dynamics at germband retraction and mid-dorsal closure

	Germband retraction		Mid-dorsal closure	
Protein	Durations	Lull times	Durations	Lull times
Zip::GFP	121.3±18.0	258.1±160.1	174.0±64.4	81.1±39.7
Sqh::GFP	113.4±32.1	287.1±158.0	123.7±32.5	113.8±49.4
MoeABD::GFP	237.4±44.2	200.0±228.3	145.8±23.1	102.0±53.9

Values are in seconds (mean ± s.d.).

1). Next, we compared their behavior using live imaging. At germband retraction, Zip::GFP networks were relatively small but moved along the long axis of the cell (Fig. 3H, arrow). They had durations of 121.3±18.0 (mean ± s.d.) seconds (5 embryos, 3-9 events from 2-5 cells, averaged per embryo), with highly variable lull times between pulses (258.1±160.1 seconds; 5 embryos, 4-6 events from 2-5 cells) (Fig. 3M; Table 2). Sqh::GFP networks had statistically indistinguishable durations (113.4±32.1 seconds; 5 embryos, 3-9 events from 3-4 cells) (Fig. 3L) and lull times (287.1±158.0 seconds; 5 embryos, 7-12 events from 2-4 cells) (Fig. 3M). F-actin networks appeared larger (Fig. 3I, white arrow), and as they moved along the length of the cell they often formed lamellipodia-like protrusions that extended over neighboring cells (Fig. 3I, yellow arrows). Moreover, the actin network durations were significantly longer than both the Zip::GFP and Sqh::GFP networks at this stage (237.4±44.2 seconds; 6 embryos, 4-5 events, each from different cells; $P<0.01$) (Fig. 3L), but lull times were statistically indistinguishable from the myosin networks and highly variable (200.0±228.3 seconds; 6 embryos, 4-5 events, each from different cells) (Fig. 3M). Thus, the actin and myosin networks have distinct properties as they first form at germband retraction; the myosin networks are presumably linked to actin, but perhaps only for a portion of an actin network lifetime.

Next, we compared the actin and myosin networks at DC. At mid-DC (with the epidermal leading edge taut, but before epidermal zippering), each network typically traversed the apical cell surface as they assembled and disassembled, but none converted into cell protrusions (Fig. 3J,K). The Zip::GFP and Sqh::GFP networks became larger (Fig. 3J), and the duration of the Zip::GFP networks increased compared with that at germband retraction: 174.0±64.4 seconds (9 embryos, 4-5 events, each from different cells) at DC versus 121.3±18.0 seconds at germband retraction (Fig. 3N versus 3L; Table 2) ($P=0.044$). By contrast, the MoeABD::GFP network durations decreased compared with those at germband retraction: 145.8±23.1 seconds (9 embryos, 4-5 events, each from different cells) at DC versus 237.4±44.2 seconds at germband retraction (Fig. 3N versus 3L) ($P<0.01$) and, as a result, overlapped with the Zip::GFP network durations (Fig. 3N). The Sqh::GFP duration times only displayed a slight and statistically insignificant increase at DC (123.7±32.5 seconds; 8 embryos, 4-6 events, each from different cells) versus germband retraction (113.4±32.1 seconds). Nonetheless, the Sqh::GFP, Zip::GFP and MoeABD::GFP duration times were statistically indistinguishable at DC. The lull times between pulses were also statistically indistinguishable among MoeABD::GFP (102.0±53.9 seconds; 5 embryos, 3-5 events, each from different cells), Zip::GFP (81.1±39.7 seconds; 6 embryos, 4-5 events, each from different cells) and Sqh::GFP (113.8±49.4 seconds; 8 embryos, 3-6 events, each from different cells), and these times were less variable than at germband retraction (Fig. 3O versus 3M). Thus, the actin and myosin networks (hereafter referred to as actomyosin networks) become closely entrained into repeated assembly/disassembly cycles at the apical surface of amnioserosa cells at DC.

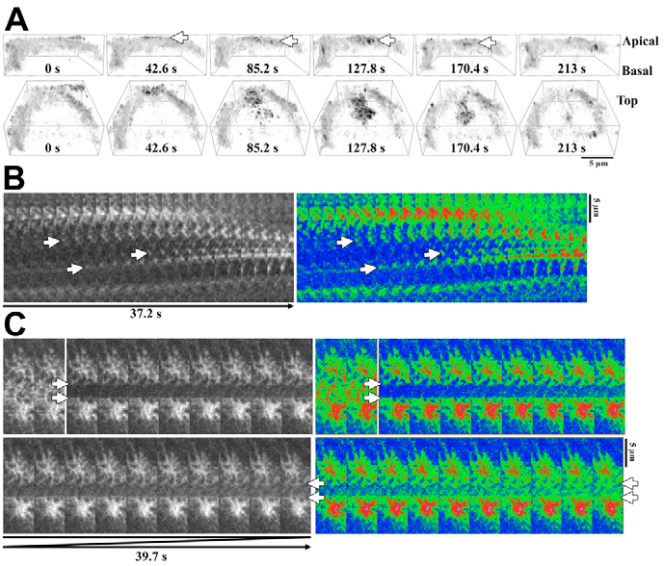

Fig. 4. Assembly of apical myosin networks. (**A**) Three-dimensional reconstructions of Sqh::GFP in a single *Drosophila* amnioserosa cell during network assembly and disassembly. Note network assembly at the apical surface (arrows). (**B**) Kymograph of Sqh::GFP network showing individual node growth (arrows). Grayscale images, left; RGB rainbow, right. (**C**) Photobleached center of an Sqh::GFP network. Note the relatively uniform recovery of node fluorescence (arrows).

To complete the developmental analysis, we analyzed Sqh::GFP at the zippering stage of DC, when cells at the canthi (the corners of the eye-shaped amnioserosa) have a much smaller apical circumference than central amnioserosa cells (Fig. 3P′). Remarkably, network durations and lull times between pulses were indistinguishable between the cells (Fig. 3P,Q). However, relative to mid-DC, network durations were slightly shorter: 114.4±14.4 seconds for central cells (6 embryos, 7-24 events from 4-5 cells) ($P=0.14$) and 100.1±16.7 seconds for canthi cells (5 embryos, 8-23 events from 3-5 cells) ($P=0.03$); and lull times between pulses were substantially shorter: 33.4±30.6 seconds for central cells (6 embryos, 10-27 events from 4-5 cells) ($P<0.01$) and 30.4±18.0 seconds for canthi cells (5 embryos, 8-21 events from 3-5 cells) ($P<0.01$). Thus, network dynamics change with development, but at any given developmental stage network dynamics are apparently independent of apical area. All analyses below are at mid-DC.

To confirm where the networks form in the cell, we analyzed three-dimensional reconstructions of single cells expressing Sqh::GFP. Top views revealed network formation and side views revealed formation specifically in the apical domain (Fig. 4A, arrows). To understand how the networks assemble, we analyzed kymographs of single Sqh::GFP networks. This showed individual nodes of the networks growing in intensity at different times (Fig. 4B, arrows). These nodes could form by the local rearrangement of a diffuse pre-existing network, the recruitment of diffusible subunits, or both. To test whether local changes could solely account for node growth, we photobleached the centers of Sqh::GFP networks as they neared full constriction. We detected recovery of fluorescent nodes evenly across the photobleached regions (Fig. 4C, arrows), indicating Sqh::GFP recruitment from other parts of the cell. Thus, assembling myosin networks are likely to incorporate diffusible subunits, although some incorporation of pre-existing networks cannot be excluded.

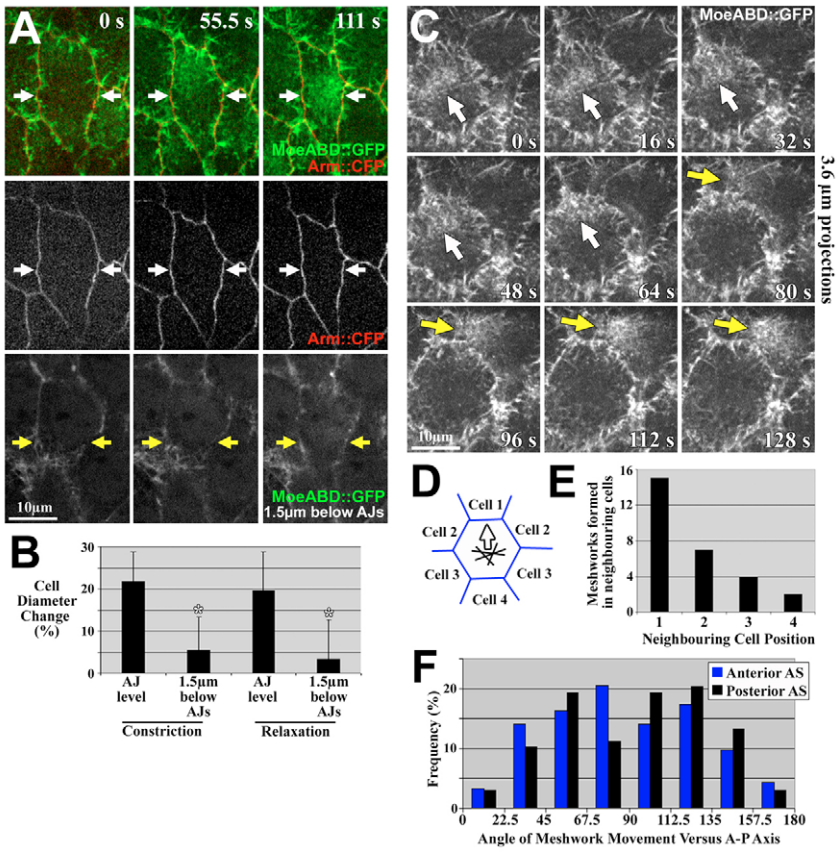

Fig. 5. The networks mediate apical constriction. (**A**) Live dual imaging of *Drosophila* amniosera cells. Top and middle rows show the same apical focal plane. Note cell constriction at adherens junctions (AJs) (Arm::CFP; arrows) with actin network (MoeABD::GFP). Bottom row shows a focal plane 1.5 μm below, where the cortex, as marked by MoeABD::GFP, is less responsive (yellow arrows). (**B**) Quantification of the change in cell diameter in response to actin networks at AJs versus the same position 1.5 μm below (n=23 events, each from different cells, from 5 embryos). Cell diameters were measured along the most-affected cell axis. Asterisks indicate significant differences (P<0.01). (**C**) Live imaging of MoeABD::GFP network disassembly in one cell (white arrows) followed by network assembly in a neighbor (yellow arrows). (**D**,**E**) Scheme for (D), and results of (E), quantifying which neighboring cell assembles a network after network disassembly at the indicated cell contact (D, arrow) (n=28 events from 8 embryos). (**F**) Network translocation angles relative to the anteroposterior embryo axis (n=92 events from 5 embryos for anterior amnioserosa; n=98 events from 5 embryos for posterior amnioserosa).

The pulsing actomyosin networks drive pulsed apical constriction

To assess whether the apical surface actomyosin networks drive amnioserosa apical constriction, we tested how network assembly and disassembly affect the apical cell circumference. Dual live imaging of MoeABD::GFP and Arm::CFP showed that apical actin network assembly coincides with cell constriction, and that network disassembly coincides with cortical relaxation (Fig. 5A; see Movie 2 in the supplementary material). Constriction and relaxation occurred specifically at the level of AJs (Fig. 5A, white arrows) and were significantly reduced 1.5 μm below (Fig. 5A, yellow arrows; Fig. 5B shows quantification of cortical constriction and relaxation at both levels). Thus, actomyosin network assembly and disassembly are linked to apical constriction and relaxation, respectively. However, for a single cycle, the degree of apical constriction (a 21.7±7.2% change in cell diameter; 23 events, one cell each from 5 embryos) was followed by an indistinguishable degree of apical relaxation (a 19.7±9.2% change in cell diameter). Overall tissue constriction must therefore be gradual.

Intriguingly, the assembly and disassembly of a network in one cell was often followed by the assembly of a network in a neighboring cell (Fig. 5C, white and yellow arrows): 30/66 networks analyzed were followed by a neighboring cell network at the next time point collected (8 MoeABD::GFP embryos scored; time points were separated by 4.84-20.21 seconds). To test whether this was non-random, we quantified which neighboring cell formed a network relative to the cell-cell contact where the original network terminated. Analyzing cell arrangements with the original network in a central cell surrounded by six neighbors, the neighbor at the contact where the network terminated was termed ‘Cell 1’, and neighbors further away were termed ‘Cells 2-4’ (Fig. 5D). The neighboring networks preferentially formed next to where the original network terminated (Cell 1), and less frequently in more distant neighbors (Fig. 5E). Since this network propagation might coordinate networks across the amnioserosa, we examined the orientation of network movements relative to the embryonic axes. We analyzed cells at both the anterior and posterior regions of the amnioserosa because they have different cell shapes (Gorfinkiel et al., 2009). For both regions, the orientation of network movement was biased towards the dorsoventral (D-V) axis of the embryo (Fig. 5F). Thus, actomyosin activity may propagate between cells to coordinate amnioserosa tissue constriction.

The actomyosin networks interact transiently with the apical PAR protein patch

To assess how PAR proteins could affect myosin, we used live imaging to evaluate PAR protein dynamics in amnioserosa cell apical domains. For Baz, we imaged a gene-trap line with GFP inserted at the *baz* locus (Baz::GFP). For Par-6, we generated a fly line with inducible Par-6::GFP. Both Baz::GFP and Par-6::GFP formed a central patch of puncta at the apical surface of amnioserosa cells at DC (Fig. 6A,B, bracketed) plus circumferential localization. In each case, although the patch showed some movement, it persisted at the apical surface (Fig. 6A,B). Dual live imaging of overexpressed Par-6::GFP and Baz::mCherry confirmed colocalization of these proteins in puncta at the apical surface (Fig. 6C, arrows), although it was only partial (Table 1). Dual live imaging of Baz::GFP and Sqh::mCherry showed the presence of apical Baz::GFP before and after myosin networks formed (Fig. 6D, brackets). Network assembly sites did not correlate with the Baz::GFP patch, but the networks inevitably traversed the patches because they covered much of the apical surface (Fig. 6D, arrow

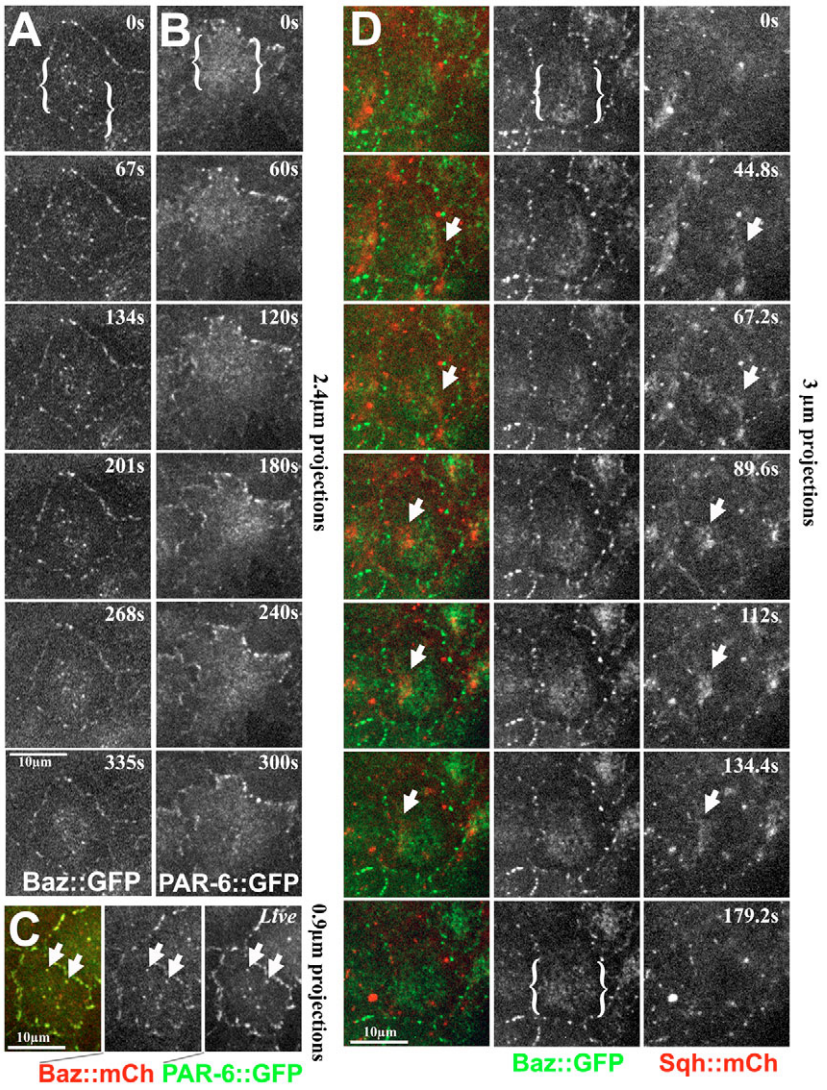

Fig. 6. Comparison of PAR complex and myosin dynamics. (**A**) *Drosophila* amniosera cells showing localization of Baz::GFP. Apical surface puncta are bracketed. (**B**) Par-6::GFP. Apical surface puncta are bracketed. (**C**) Dual live imaging of Baz::mCherry and Par-6::GFP. Some apical surface puncta colocalize (arrows). (**D**) Dual live imaging showing how the Sqh::mCherry network translocates across the Baz::GFP patch (arrows). The Baz::GFP patch is present before and after the network assembles (brackets).

marks myosin network; see Movie 3 in the supplementary material). Dual live imaging of Par-6::GFP and Sqh::mCherry showed a similar relationship (data not shown). Quantification revealed low local colocalization of Baz::GFP or Par-6::GFP with Sqh::mCherry when the PAR protein patches and myosin networks overlapped in the apical domain (Table 1). Thus, the apical PAR complexes are not core components of the actomyosin networks. Instead, they persist at the apical domain and associate transiently with the pulsing networks.

Baz and Par-6/aPKC affect different phases of the actomyosin assembly/disassembly cycle

To test how PAR complex components affect the actomyosin networks, we first imaged Zip::GFP in zygotic homozygous mutants for baz^{Xi106}, $par\text{-}6^{\Delta 226}$ or $aPKC^{K06403}$ at mid-DC. Networks formed of apparently normal size and structure in each case (Fig. 7A,B,D,E). Since Baz protein is undetectable in baz^{Xi106} zygotic mutants at this stage (Tanentzapf and Tepass, 2003) (our unpublished observations), network formation might be independent of Baz. We cannot conclude the same for Par-6 or aPKC because of the maternally inherited gene product present in *par-6* and *aPKC* mutants (data not shown). We noted 8/21 *baz* mutant embryos and 5/16 *par-6* mutant embryos with amnioserosa morphological defects in Zip::GFP live imaging (Fig. 7C,F, yellow arrows). Myosin networks still formed (Fig. 7C,F, white arrows) and pulsed, but to discount possible non-specific effects of tissue disruption we excluded these embryos from the analyses below. No *aPKC* mutants displayed amnioserosa morphological defects.

To test whether the networks pulse normally in the mutants we quantified pulse durations, lull times between pulses and overall pulse frequencies. Duration times in *par-6* and *aPKC* mutants were indistinguishable from that of controls with equal dosage of Zip::GFP, but *baz* mutants had significantly shorter duration times (117.9±11.4 seconds; 8 embryos, 11-30 events from 6-10 cells) than controls (153.0±19.7 seconds; 7 embryos, 13-28 events from 5-12 cells) ($P<0.01$) (Fig. 7G). By contrast, *par-6* and *baz* mutant lull times were indistinguishable from those of controls, but *aPKC* mutant lull times were significantly shorter (39.0±31.4 seconds; 7 embryos, 7-30 events from 3-9 cells) than in controls (110.3±48.2 seconds; 7 embryos, 11-33 events from 5-12 cells) ($P<0.01$) (Fig. 7H). Pulses per 10 minutes for *par-6* and *baz* mutants were also indistinguishable from those of controls, but *aPKC* mutants had significantly more frequent pulses (3.98±1.09 pulses per cell per 10 minutes; 7 embryos, 3-9 cells) than controls (2.65±0.55 pulses per cell per 10 minutes; 6 embryos, 7-14 cells) ($P=0.0196$) (Fig. 7I). These results suggest a separation of PAR protein function, with Baz

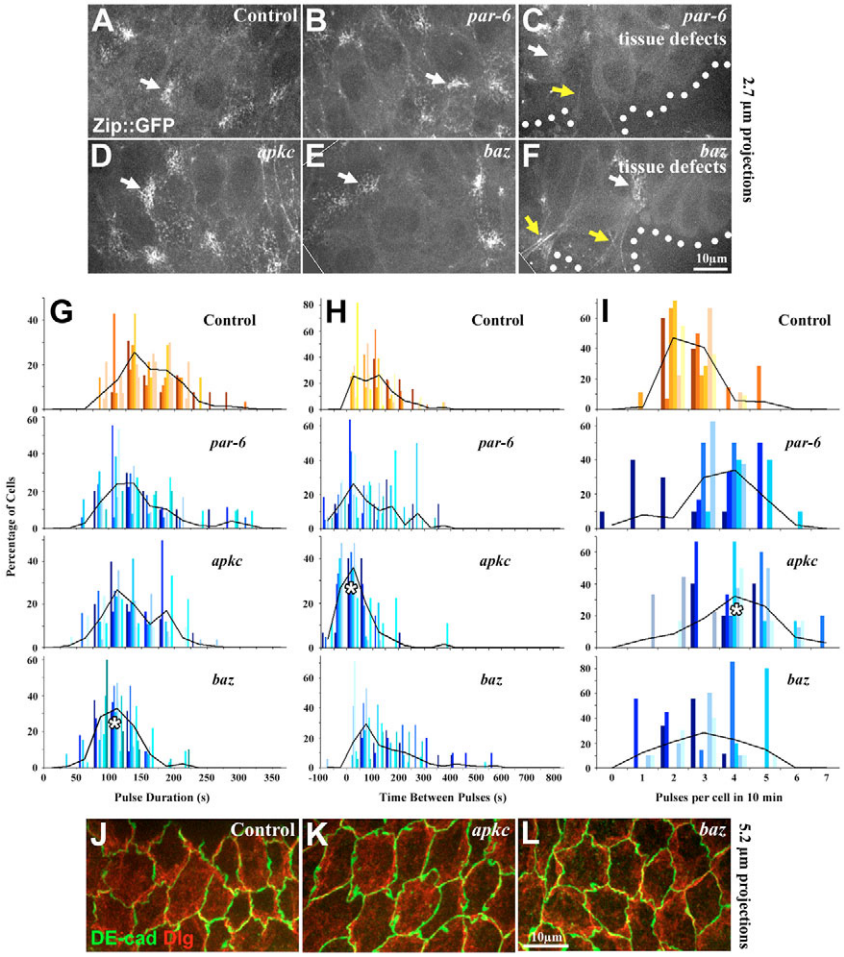

Fig. 7. Effects of PAR complex loss of function on myosin. (**A-F**) Zip::GFP localization in *Drosophila par-6* (B,C), *aPKC* (D) and *baz* (E,F) single zygotic mutants compared with control with equal Zip::GFP dosage (A). White arrows indicate myosin networks. Yellow arrows indicate myosin fibers associated with tissue holes (outlined). (**G-I**) Comparison of Zip::GFP network durations (G), lull time between pulses (H) and pulses per 10 minutes (I) between *par-6*, *aPKC* and *baz* single zygotic mutants and control. For each bar chart, each color describes the distribution of one embryo and the black line is the average distribution of all embryos. Asterisks indicate significant differences ($P<0.05$). (**J-L**) DE-Cad and Dlg in *aPKC* (K) and *baz* (L) single zygotic mutants and control (J).

promoting pulse durations and aPKC promoting lull times between pulses. Importantly, *aPKC* mutants had normal apicobasal polarity and AJs [DE-Cad and Discs large (Dlg) staining; 12/12 embryos analyzed; Fig. 7K] as in controls (6/6 embryos analyzed; Fig. 7J). Consistent with our Zip::GFP live imaging, 4/13 *baz* mutants showed amnioserosa morphology defects with DE-Cad and Dlg staining, but *baz* mutants with normal morphology had normal apicobasal polarity and AJs (Fig. 7L). Thus, the effects on myosin occur without general epithelial defects.

Separation of function suggests separate PAR protein localization mechanisms. Indeed, in *baz* zygotic mutants, we detected aPKC apically in both epidermal and amnioserosa cells despite undetectable Baz (data not shown). Thus, aPKC might be able to regulate lull times without Baz. We detected both Baz and aPKC in *aPKC* mutants (data not shown), preventing conclusions about Baz function in the absence of aPKC.

Next, we evaluated Zip::GFP with PAR gene overexpression targeted to the amnioserosa. Overexpressing untagged Par-6 or membrane-targeted aPKC (aPKC-CAAX) had no significant effects alone (Fig. 8A-C). However, co-overexpressing Par-6 plus aPKC-CAAX significantly reduced network pulse frequency (2.05±0.52 pulses per cell per 20 minutes; 5 embryos, 7-11 cells) versus controls with equal dosage of Zip::GFP (5.81±2.11 pulses per cell per 20 minutes; 5 embryos, 5-11 cells) (P=0.014) (Fig. 8C). Lull times were also significantly higher than in controls (P=0.04), and had a wide variation (Fig. 8B). However, pulse durations were statistically indistinguishable from those of controls (Fig. 8A).

Next, we overexpressed untagged Baz. This significantly increased duration times (189.8±17.1 seconds; 6 embryos, 22-60 events from 6-13 cells) versus controls (108.3±31.2 seconds; 5 embryos, 9-45 events from 5-12 cells) (P<0.01) (Fig. 8A) and decreased lull times between pulses (28.7±14.2 seconds; 6 embryos, 22-60 events from 6-13 cells) versus controls (108.3±31.2 seconds; 5 embryos, 9-45 events from 5-12 cells) (P=0.04) (Fig. 8B), and, as a result, had no statistically significant effect on pulse frequency versus controls (Fig. 8C). Myosin networks were of apparently normal size and structure with Par-6 plus aPKC-CAAX overexpression or Baz overexpression as compared with controls (Fig. 8D-F, arrows), although some cells with Par-6 plus aPKC-CAAX overexpression never formed networks (Fig. 8C) and had lower overall Zip::GFP levels (Fig. 8E, outlined). Dlg and DE-Cad staining showed normal apicobasal polarity and AJs in controls (10/10 embryos) and in most embryos overexpressing Par-6 plus aPKC-CAAX (12/19) or overexpressing Baz (14/16) (Fig. 8G-I). Although a portion of Par-6 plus aPKC-CAAX-overexpressing embryos and Baz-overexpressing embryos displayed AJ fragmentation, all embryos analyzed had effects on Zip::GFP dynamics. Thus, defects in myosin dynamics were more prevalent than defects in epithelial structure, arguing in favor of more direct effects on myosin. These data further indicate that Par-6/aPKC and Baz have distinct effects on myosin pulses, with Par-6/aPKC promoting lull times and Baz promoting network durations. Baz overexpression also decreased lull times, which might result from the increase in pulse durations or more direct effects on the lull phase.

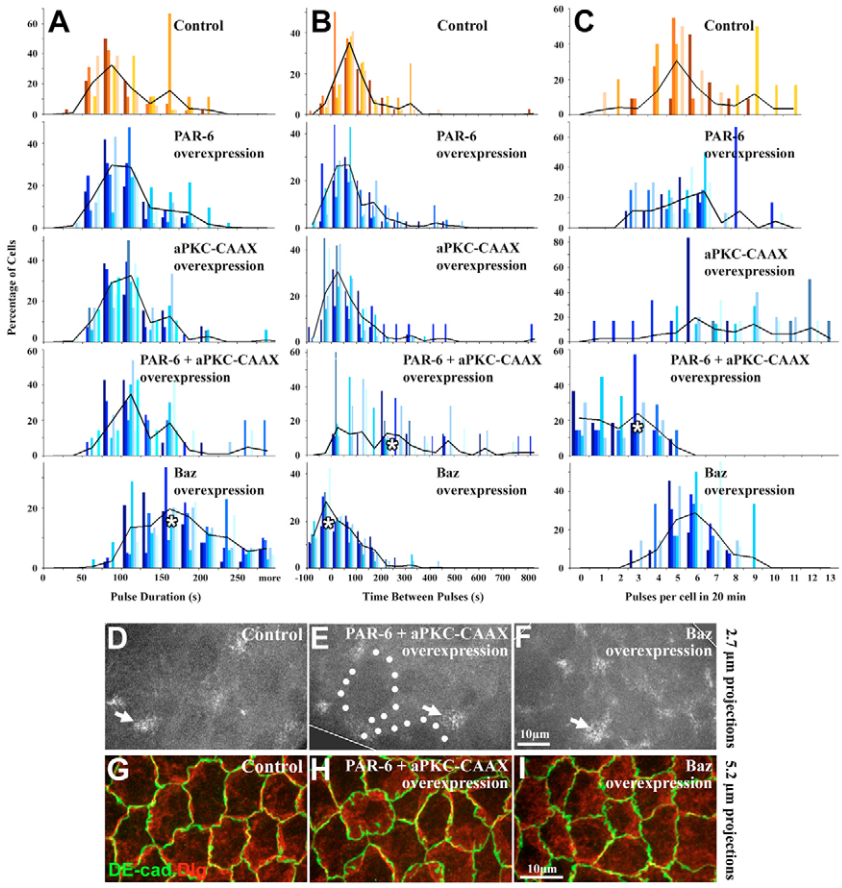

Fig. 8. Effects of PAR complex gain of function on myosin. (**A-C**) Zip::GFP network durations (A), lull times between pulses (B) and pulses per 10 minutes (C) in *Drosophila* embryos overexpressing Par-6, aPKC-CAAX, Par-6 plus aPKC-CAAX, or Baz, compared with control with equal Zip::GFP dosage. For each bar chart, each color describes the distribution of one embryo and the black line is the average distribution of all embryos. Asterisks indicate significant differences (P<0.05). (**D-F**) Zip::GFP localization with Par-6 plus aPKC-CAAX overexpression (E) or Baz overexpression (F) compared with control (D). White arrows indicate myosin networks. Cells with reduced myosin levels are outlined. (**G-I**) DE-Cad (green) and Dlg (red) with Par-6 plus aPKC-CAAX overexpression (H) or Baz overexpression (I) compared with control (G).

To test whether amnioserosa-targeted PAR protein overexpression affects DC, we measured the rate of change in amnioserosa diameter at the center of the tissue, from one epidermal leading edge to the other, over DC in embryos with the same dosage of Zip::GFP (see Fig. S1A in the supplementary material). Control, Par-6 plus aPKC-CAAX-overexpressing and Baz-overexpressing embryos had relatively linear DC rates (see Fig. S1B-D in the supplementary material). For quantification, we generated lines of best fit for each embryo centered at 50 µm diameter and extending ±60 minutes. Control DC rates (5.3±1.5 nm/second; 5 embryos) were statistically indistinguishable from those of PAR protein-overexpressing embryos, but DC was faster with Baz overexpression (7.0±1.2 nm/second; 6 embryos) than with Par-6 plus aPKC-CAAX overexpression (4.0±2.5 nm/second; 7 embryos) (P=0.028).

DISCUSSION

Pulsing actomyosin networks and amnioserosa apical constriction

The repeated assembly and disassembly of apical actomyosin networks is an integral part of amnioserosa tissue morphogenesis during DC. Restricting myosin to the amnioserosa alone is sufficient for amnioserosa apical constriction and overall DC (Franke et al., 2005). Franke et al. also described ‘dynamic’ apical myosin in the amnioserosa (Franke et al., 2005). We defined these dynamics as repeated assembly and disassembly cycles of actomyosin networks. Moreover, assembly and disassembly are linked to apical constriction and relaxation, respectively. This is consistent with laser ablation studies showing that the apical surfaces of amnioserosa cells maintain tension across the tissue (Ma et al., 2009). Moreover, AJ live imaging has revealed general pulsing of amnioserosa cells from germband retraction through DC (Solon et al., 2009). The pulsing actomyosin networks arise with this same developmental timing. Solon et al. (Solon et al., 2009) observed a 230±76 second periodicity of cortical pulsing at DC, similar to that of the pulsing actomyosin networks. We find that increased network durations and decreased lull times with amnioserosa-targeted Baz overexpression coincide with faster DC, as compared with amnioserosa-targeted Par-6 plus aPKC-CAAX overexpression, which increases lull times. We conclude that the pulsing actomyosin networks mediate the constriction of individual amnioserosa cells and that this contributes to DC.

Remarkably, a single amnioserosa apical constriction event is followed by an almost equal relaxation (Fig. 3). However, over many constrictions the cells progressively reduce their apical surface area (Solon et al., 2009). This suggests that ratcheting mechanisms incrementally harness the constrictions for overall tissue change. Intracellular and extracellular ratchets are possible. Cells of the *Drosophila* ventral furrow also display pulsed contractions of apical actomyosin networks as they apically constrict (Martin et al., 2009). However, there is minimal relaxation after each constriction. Instead, residual myosin filaments are retained between pulses, and may act as intracellular ratchets to harness the pulsed contractions (Martin et al., 2009). By contrast, we rarely observed residual myosin filaments between actomyosin pulses in amnioserosa cells, possibly explaining their relaxation after each cell constriction. Solon et al. proposed that the leading edge actomyosin cable of the surrounding epidermis acts as an extracellular ratchet to harness amnioserosa contractility (Solon et al., 2009). However, the ability of myosin expression in the amnioserosa alone to drive DC (Franke

et al., 2005) suggests that other mechanisms contribute. Indeed, DC is a robust process with redundant contributions from both amnioserosa and epidermis (Franke et al., 2005; Kiehart et al., 2000). At later stages, filopodia-based epidermal zippering at the canthi could provide another extracellular ratchet (Gorfinkiel et al., 2009). In addition, each amnioserosa cell has a persistent circumferential actin belt that might act as an intracellular ratchet, and other uncharacterized processes, such as membrane trafficking or basal activities, could also contribute.

Actomyosin activity also appears to be linked between cells. The networks display preferential D-V movement, and a network in one cell appears to promote network formation in neighbors. Overall amnioserosa cell shape changes are also coordinated between neighbors (Solon et al., 2009). Moreover, myosin activity in isolated amnioserosa cells can elicit cortical myosin accumulation in neighboring epidermal cells (Franke et al., 2005). We speculate that feedback from epidermal cells might orient the D-V movement of amnioserosa actomyosin networks. Interestingly, amnioserosa cells also preferentially contract along the D-V axis (Gorfinkiel et al., 2009). Although the actomyosin networks move in this direction, it is unlikely that they are solely responsible for the directional cell shape changes – the networks affect the cell circumference both along the axis of their trajectory and perpendicular to it, and, as discussed, both effects are transient. Thus, forces from the epidermis might be needed for the biased D-V amnioserosa cell contraction, and they might also direct the D-V movement of amnioserosa actomyosin networks to facilitate DC.

Regulation of the actomyosin networks by the PAR complex

As the actomyosin networks assemble and disassemble, they translocate across a persistent PAR protein patch. These transient associations and lack of specific colocalization between the actomyosin networks and the PAR proteins argue against PAR proteins being integral parts of the actomyosin networks. However, our results show that the PAR proteins regulate the networks. Our genetic interaction tests indicate that Baz, Par-6 and aPKC support myosin activity for proper DC. Strikingly, the live imaging revealed that Baz and Par-6/aPKC regulate distinct phases of the myosin assembly/disassembly cycle. Together, our loss-of-function and gain-of-function studies show that Baz promotes network durations, whereas Par-6 and aPKC promote lull times between pulses. Baz overexpression also decreased lull times, which could result indirectly from increased network durations or from more direct inhibition of the lull phase. Importantly, our overexpression experiments indicate that the effects occur specifically in amnioserosa cells, and analyses of cell polarity and AJs indicate that the PAR proteins have relatively direct effects on the actomyosin networks. However, it remains possible that the PAR proteins have additional functions in the amnioserosa.

A number of molecular interactions must control PAR protein activity in the apical domain of amnioserosa cells. The PAR proteins often, but not exclusively, colocalize in amnioserosa cells, suggesting a dynamic relationship consistent with separate Baz and Par-6/aPKC functions. They also show colocalization with Crb, an apical transmembrane protein at the core of the Crb polarity complex (reviewed by Tepass et al., 2001). Interestingly, Crb is known to regulate DC (Harden et al., 2002), and Par-6 and aPKC can bind Crb complex components (Nam and Choi, 2003; Sotillos et al., 2004). Thus, Crb might be one anchor for PAR proteins at the apical surface of amnioserosa cells.

Molecular mechanisms connecting PAR proteins to myosin and actin have been implicated in a number of studies. For example, aPKC phosphorylates and inhibits mammalian myosin IIB (Even-Faitelson and Ravid, 2006), although these sites are not present in *Drosophila* Myosin II (Zipper). Par-6/aPKC also inhibits Rho by activating the ubiquitin ligase Smurf1 in mammalian cells (Ozdamar et al., 2005; Wang et al., 2003). Additionally, Baz and aPKC immunoprecipitate with Sqh from *Drosophila* egg chambers (Wang and Riechmann, 2007). Analogous to amnioserosa morphogenesis, mammalian Par-3 and Par-6/aPKC regulate distinct aspects of cell shape change through different cytoskeletal regulators during dendritic spine morphogenesis: Par-3 inhibits cell protrusions by inhibiting Rac through sequestering the RacGEF Tiam1 (Chen and Macara, 2005; Zhang and Macara, 2006), whereas Par-6/aPKC promotes protrusions by inhibiting Rho via p190 RhoGAP (Zhang and Macara, 2008).

Amnioserosa cell apical constriction has similarities to endoderm precursor cell apical constriction during *C. elegans* gastrulation. Here, myosin activity drives cell ingression (Lee and Goldstein, 2003). Similar to in amnioserosa cells, the PAR complex and myosin accumulate at the center of the apical surface of these cells (Nance and Priess, 2002) and of earlier cells as well (Munro et al., 2004). However, these *C. elegans* actomyosin networks do not appear to undergo full assembly/disassembly cycles and instead progressively accumulate (Nance et al., 2003) or display continual network flows (Munro et al., 2004). Interestingly, apical myosin enrichment requires PAR-3 in *C. elegans* endodermal precursor cells (Nance et al., 2003). Apical myosin enrichment also requires Baz, Par-6 and aPKC in *Drosophila* egg chamber follicle cells (Wang and Riechmann, 2007). These results suggest that the PAR complex initiates actomyosin network assembly, contrasting with the amnioserosa, in which networks can assemble without detectable Baz and are inhibited by Par-6/aPKC. Perhaps, actomyosin networks with full assembly/disassembly cycles are regulated distinctly. In the one-cell *C. elegans* embryo, PAR protein puncta move with a multifaceted cortical myosin network to the embryo anterior (Munro et al., 2004). Each facet of the network assembles and disassembles with durations similar to those of the amnioserosa actomyosin networks. The network can also form without the PAR proteins, but the overall flow of the network fails with loss of PAR-3, PAR-6 or aPKC (Munro et al., 2004). It would be interesting to test whether PAR-3, PAR-6 and aPKC have distinct effects on the individual facets of these networks.

Other regulators of the actomyosin assembly/disassembly cycle

What triggers actomyosin network assembly in amnioserosa cells? It appears to be independent of Baz, and must overcome Par-6/aPKC inhibition. The Rho pathway triggers actomyosin contractility in many contexts (reviewed by Lecuit and Lenne, 2007; Matsumura, 2005; Raftopoulou and Hall, 2004). However, amnioserosa-targeted expression of dominant-negative Rho does not appear to block DC (Harden et al., 2002). Alternatively, actin assembly might trigger the networks. Actin networks appear larger and last longer than myosin networks as both start forming during germband retraction. This suggests that actin might organize these networks during germband retraction and possibly DC. Intriguingly, Rac inhibition disrupts DC and reduces amnioserosa actin levels (Harden et al., 2002). The trigger might also involve intercellular forces from networks in neighboring cells.

How is the actomyosin assembly/disassembly periodicity regulated? Since we rarely observed more than one network per cell, network assembly might require disassembly of the existing network.

Disassembly might begin a cascade that ultimately triggers formation of the next network. For cycling, assembly might likewise elicit disassembly. Our data indicate that the PAR proteins are important elements of the regulatory network that is involved. Once a network is triggered, Baz prolongs it, but as the network persists, trigger and maintenance signals must be overcome for network disassembly. With disassembly, Par-6/aPKC activity appears to inhibit new assembly, promoting lull times. With time, this Par-6/aPKC activity must diminish and/or be overwhelmed by the trigger mechanism for new network assembly to occur. Identifying trigger and feedback mechanisms within this cycle will be key for understanding how pulsed actomyosin contractions are regulated in the amnioserosa.

Acknowledgements
We thank J. Brill and U. Tepass for discussions; D. Godt and R. Winklbauer for critiques of the manuscript; C. Yu for technical assistance; C. Doe, D. Montell, M. Peifer, M. Pellikka, U. Tepass, A. Wodarz, J. Zallen, the BDSC, FlyTrap and the DSHB for reagents. A.T. was awarded a University of Toronto Excellence Award for Undergraduate Research. This work was supported by an NSERC Discovery Grant to T.J.C.H. T.J.C.H. holds a Tier II Canada Research Chair.

Competing interests statement
The authors declare no competing financial interests.

Supplementary material
Supplementary material for this article is available at
http://dev.biologists.org/lookup/suppl/doi:10.1242/dev.044107/-/DC1

References

Chen, X. and Macara, I. G. (2005). Par-3 controls tight junction assembly through the Rac exchange factor Tiam1. *Nat. Cell Biol.* **7**, 262-269.
Cowan, C. R. and Hyman, A. A. (2007). Acto-myosin reorganization and PAR polarity in C. elegans. *Development* **134**, 1035-1043.
Even-Faitelson, L. and Ravid, S. (2006). PAK1 and aPKCzeta regulate myosin II-B phosphorylation: a novel signaling pathway regulating filament assembly. *Mol. Biol. Cell* **17**, 2869-2881.
Franke, J. D., Montague, R. A. and Kiehart, D. P. (2005). Nonmuscle myosin II generates forces that transmit tension and drive contraction in multiple tissues during dorsal closure. *Curr. Biol.* **15**, 2208-2221.
Goldstein, B. and Macara, I. G. (2007). The PAR proteins: fundamental players in animal cell polarization. *Dev. Cell* **13**, 609-622.
Gorfinkiel, N., Blanchard, G. B., Adams, R. J. and Martinez Arias, A. (2009). Mechanical control of global cell behaviour during dorsal closure in Drosophila. *Development* **136**, 1889-1898.
Harden, N. (2002). Signaling pathways directing the movement and fusion of epithelial sheets: lessons from dorsal closure in Drosophila. *Differentiation* **70**, 181-203.
Harden, N., Ricos, M., Yee, K., Sanny, J., Langmann, C., Yu, H., Chia, W. and Lim, L. (2002). Drac1 and Crumbs participate in amnioserosa morphogenesis during dorsal closure in Drosophila. *J. Cell Sci.* **115**, 2119-2129.
Jacinto, A., Woolner, S. and Martin, P. (2002). Dynamic analysis of dorsal closure in Drosophila: from genetics to cell biology. *Dev. Cell* **3**, 9-19.
Kiehart, D. P., Galbraith, C. G., Edwards, K. A., Rickoll, W. L. and Montague, R. A. (2000). Multiple forces contribute to cell sheet morphogenesis for dorsal closure in Drosophila. *J. Cell Biol.* **149**, 471-490.
Lecuit, T. and Lenne, P. F. (2007). Cell surface mechanics and the control of cell shape, tissue patterns and morphogenesis. *Nat. Rev. Mol. Cell Biol.* **8**, 633-644.
Lee, J. Y. and Goldstein, B. (2003). Mechanisms of cell positioning during C. elegans gastrulation. *Development* **130**, 307-320.
Ma, X., Lynch, H. E., Scully, P. C. and Hutson, M. S. (2009). Probing embryonic tissue mechanics with laser hole drilling. *Phys. Biol.* **6**, 036004.
Martin, A. C., Kaschube, M. and Wieschaus, E. F. (2009). Pulsed contractions of an actin-myosin network drive apical constriction. *Nature* **457**, 495-499.
Matsumura, F. (2005). Regulation of myosin II during cytokinesis in higher eukaryotes. *Trends Cell Biol.* **15**, 371-377.
McGill, M. A., McKinley, R. F. and Harris, T. J. (2009). Independent cadherin-catenin and Bazooka clusters interact to assemble adherens junctions. *J. Cell Biol.* **185**, 787-796.
Munro, E. M. (2006). PAR proteins and the cytoskeleton: a marriage of equals. *Curr. Opin. Cell Biol.* **18**, 86-94.
Munro, E., Nance, J. and Priess, J. R. (2004). Cortical flows powered by asymmetrical contraction transport PAR proteins to establish and maintain anterior-posterior polarity in the early C. elegans embryo. *Dev. Cell* **7**, 413-424.
Nam, S. C. and Choi, K. W. (2003). Interaction of Par-6 and Crumbs complexes is essential for photoreceptor morphogenesis in Drosophila. *Development* **130**, 4363-4372.
Nance, J. and Priess, J. R. (2002). Cell polarity and gastrulation in C. elegans. *Development* **129**, 387-397.
Nance, J., Munro, E. M. and Priess, J. R. (2003). C. elegans PAR-3 and PAR-6 are required for apicobasal asymmetries associated with cell adhesion and gastrulation. *Development* **130**, 5339-5350.
Ozdamar, B., Bose, R., Barrios-Rodiles, M., Wang, H. R., Zhang, Y. and Wrana, J. L. (2005). Regulation of the polarity protein Par6 by TGFbeta receptors controls epithelial cell plasticity. *Science* **307**, 1603-1609.
Pinheiro, E. M. and Montell, D. J. (2004). Requirement for Par-6 and Bazooka in Drosophila border cell migration. *Development* **131**, 5243-5251.
Pope, K. L. and Harris, T. J. (2008). Control of cell flattening and junctional remodeling during squamous epithelial morphogenesis in Drosophila. *Development* **135**, 2227-2238.
Raftopoulou, M. and Hall, A. (2004). Cell migration: Rho GTPases lead the way. *Dev. Biol.* **265**, 23-32.
Rodriguez-Diaz, A., Toyama, Y., Abravanel, D. L., Wiemann, J. M., Wells, A. R., Tulu, U. S., Edwards, G. S. and Kiehart, D. P. (2008). Actomyosin purse strings: renewable resources that make morphogenesis robust and resilient. *HFSP J.* **2**, 220-237.
Royou, A., Sullivan, W. and Karess, R. (2002). Cortical recruitment of nonmuscle myosin II in early syncytial Drosophila embryos: its role in nuclear axial expansion and its regulation by Cdc2 activity. *J. Cell Biol.* **158**, 127-137.
Simske, J. S. and Hardin, J. (2001). Getting into shape: epidermal morphogenesis in Caenorhabditis elegans embryos. *BioEssays* **23**, 12-23.
Skoglund, P., Rolo, A., Chen, X., Gumbiner, B. M. and Keller, R. (2008). Convergence and extension at gastrulation require a myosin IIB-dependent cortical actin network. *Development* **135**, 2435-2444.
Solon, J., Kaya-Copur, A., Colombelli, J. and Brunner, D. (2009). Pulsed forces timed by a ratchet-like mechanism drive directed tissue movement during dorsal closure. *Cell* **137**, 1331-1342.
Sotillos, S., Diaz-Meco, M. T., Caminero, E., Moscat, J. and Campuzano, S. (2004). DaPKC-dependent phosphorylation of Crumbs is required for epithelial cell polarity in Drosophila. *J. Cell Biol.* **166**, 549-557.
Suzuki, A. and Ohno, S. (2006). The PAR-aPKC system: lessons in polarity. *J. Cell Sci.* **119**, 979-987.
Tanentzapf, G. and Tepass, U. (2003). Interactions between the crumbs, lethal giant larvae and bazooka pathways in epithelial polarization. *Nat. Cell Biol.* **5**, 46-52.
Tepass, U., Tanentzapf, G., Ward, R. and Fehon, R. (2001). Epithelial cell polarity and cell junctions in Drosophila. *Annu. Rev. Genet.* **35**, 747-784.
Wang, H. R., Zhang, Y., Ozdamar, B., Ogunjimi, A. A., Alexandrova, E., Thomsen, G. H. and Wrana, J. L. (2003). Regulation of cell polarity and protrusion formation by targeting RhoA for degradation. *Science* **302**, 1775-1779.
Wang, Y. and Riechmann, V. (2007). The role of the actomyosin cytoskeleton in coordination of tissue growth during Drosophila oogenesis. *Curr. Biol.* **17**, 1349-1355.
Wiggin, G. R., Fawcett, J. P. and Pawson, T. (2005). Polarity proteins in axon specification and synaptogenesis. *Dev. Cell* **8**, 803-816.
Wodarz, A. and Nathke, I. (2007). Cell polarity in development and cancer. *Nat. Cell Biol.* **9**, 1016-1024.
Wodarz, A., Ramrath, A., Grimm, A. and Knust, E. (2000). Drosophila atypical protein kinase C associates with Bazooka and controls polarity of epithelia and neuroblasts. *J. Cell Biol.* **150**, 1361-1374.
Zallen, J. A. (2007). Planar polarity and tissue morphogenesis. *Cell* **129**, 1051-1063.
Zallen, J. A. and Wieschaus, E. (2004). Patterned gene expression directs bipolar planar polarity in Drosophila. *Dev. Cell* **6**, 343-355.
Zhang, H. and Macara, I. G. (2006). The polarity protein PAR-3 and TIAM1 cooperate in dendritic spine morphogenesis. *Nat. Cell Biol.* **8**, 227-237.
Zhang, H. and Macara, I. G. (2008). The PAR-6 polarity protein regulates dendritic spine morphogenesis through p190 RhoGAP and the Rho GTPase. *Dev. Cell* **14**, 216-226.